Synchronization in populations of electrochemical bursting oscillators with chaotic slow dynamics

Cite as: Chaos **31**, 053125 (2021); https://doi.org/10.1063/5.0041488
Submitted: 23 December 2020 . Accepted: 27 April 2021 . Published Online: 19 May 2021

Luciano A. Magrini, Margarete Oliveira Domingues, Elbert E. N. Macau, and István Z. Kiss

Synchronization in populations of electrochemical bursting oscillators with chaotic slow dynamics

Cite as: Chaos **31**, 053125 (2021); doi: 10.1063/5.0041488
Submitted: 23 December 2020 · Accepted: 27 April 2021 ·
Published Online: 19 May 2021

Luciano A. Magrini,[1,a] Margarete Oliveira Domingues,[2,b] Elbert E. N. Macau,[3,c] and István Z. Kiss[4,d]

AFFILIATIONS

[1]Federal Institute of Education, Science and Technology of São Paulo (IFSP), Votuporanga 15503-110, Brazil
[2]National Institute for Space Research (INPE), São José dos Campos 12227-010, Brazil
[3]Federal University of São Paulo at São José dos Campos (UNIFESP), São José dos Campos 12231-280, Brazil
[4]Department of Chemistry, Saint Louis University, 3501 Laclede Ave., St Louis, Missouri 63103, USA

[a]**Author to whom correspondence should be addressed:** magrini@ifsp.edu.br
[b]margarete.domingues@inpe.br
[c]elbert.macau@unifesp.br
[d]izkiss@slu.edu

ABSTRACT

We investigate the synchronization of coupled electrochemical bursting oscillators using the electrodissolution of iron in sulfuric acid. The dynamics of a single oscillator consisted of slow chaotic oscillations interrupted by a burst of fast spiking, generating a multiple time-scale dynamical system. A wavelet analysis first decomposed the time series data from each oscillator into a fast and a slow component, and the corresponding phases were also obtained. The phase synchronization of the fast and slow dynamics was analyzed as a function of electrical coupling imposed by an external coupling resistance. For two oscillators, a progressive transition was observed: With increasing coupling strength, first, the fast bursting intervals overlapped, which was followed by synchronization of the fast spiking, and finally, the slow chaotic oscillations synchronized. With a population of globally coupled 25 oscillators, the coupling eliminated the fast dynamics, and only the synchronization of the slow dynamics can be observed. The results demonstrated the complexities of synchronization with bursting oscillations that could be useful in other systems with multiple time-scale dynamics, in particular, in neuronal networks.

Oscillatory systems are characterized by underlying timescales (e.g., period); when such systems interact through coupling, small heterogeneities (i.e., different periods) can be suppressed through synchronization. Here, we considered laboratory experiments with the dissolution of iron wires in sulfuric acid. For each wire, the dissolution rate can exhibit oscillations with two very different timescales: Relatively slow chaotic oscillations are suddenly interrupted by a burst of very fast spiking. The synchronization of this very complex system was analyzed to reveal alignments of the bursting intervals and the synchronization of the oscillations of the corresponding timescales.

I. INTRODUCTION

Synchronization phenomenon has been reported and investigated in several areas[1–4] and manifests itself in different ways. Initially, for chaotic oscillators, the main interest was complete synchronization,[5,6] a situation in which two or more relatively strongly coupled oscillators exhibit identical variations in the time domain. However, at weaker coupling strengths, phase synchronization (PS) can also occur; PS is a weaker form of synchronization, in which the phase differences are bounded, although the evolution of the amplitudes over time can remain independent.[4,7] Characterization of PS requires a phase assignment to the chaotic process.

For periodic oscillators, the phase variable $\phi(t)$ is assigned considering a monotonic increment equal to 2π for each full period observed during the temporal evolution. For chaotic oscillators, the phase variable $\phi(t)$ is considered the variable directly related to the zero Lyapunov exponent of the attractor.[4] As an analogy to periodic oscillators, the Poincaré section can be applied as a phase marker for chaotic oscillators, but other techniques are also available, e.g., projection in the phase space,[8,9] Hilbert transform,[10] or continuous/discrete wavelet transforms.[11–14]

In many applications, e.g., in lasers, Faraday waves, climate models, and biological and chemical systems, the oscillations exhibit multiple timescales,[15–24] and thus, these systems belong to multiple time-scale dynamical systems (MTSDS). In the simplest example, there are two different timescales, a fast and a slow. The slow dynamics is characterized by periodic or chaotic oscillations, which displays the longest wavelengths when compared with the typical oscillations of the fast dynamics that can exhibit isolated firings (spike) or firing sets (bursting) that are interrupted by the slow dynamics.

The characterization of synchronization between coupled MTSDS-type oscillators is a difficult problem; the different timescales can synchronize differently, and thus, a single phase variable could not be used for characterization of PS.[25] Furthermore, while to synchronization of the slow dynamics can be described as with the phase coherent oscillators, the fast dynamics can synchronize in two different ways: The bursting synchronization occurs when the respective burstings exhibit the same number of spikes even when the spikes be asynchronous, and the spike synchronization occurs when bursting synchronization and synchronous spike patterns are jointly observed.[23–27]

The characterization of MTSDS synchronization could be facilitated if, in general, the different timescales could be separated. Wavelet transforms provide an excellent for filtering, time-scale separations,[18,28] and phase assignment of the complex systems using the Discrete Wavelet Complex Approach[14,29] (DWCA).

In this paper, we investigate the synchronization of coupled electrochemical MTSDS-type oscillators. Iron electrodissolution in sulfuric acid exhibits chaotic slow dynamics interrupted by fast periodic spiking as measured by the current $I(t)$ (or the rate) of the dissolution process at constant circuit potential.[18] Previously, it was demonstrated that Continuous Wavelet Transform (CWT) can effectively separate the slow and fast dynamics.[30] Here, the synchronization transitions with 2 and 25 (globally) coupled oscillators are analyzed. The experiments are performed with different coupling strengths, and the extent of phase synchronization of the slow and fast subsystems is calculated.

This article is organized as follows. Section II describes the experimental setup and the numerical methods based on wavelet transforms used in the phase assignment. The methodology for the characterization of synchronization for the slow and fast subsystems is described in Sec. III. In Sec. IV, the results are shown, separately for 2 and 25 oscillator setups. Last, Sec. V contains the conclusions.

II. EXPERIMENTAL TECHNIQUES AND NUMERICAL METHODS

This section describes the experimental setup that was used to generate the data sets and the numerical methods used in the phase assignment.

A. Experimental data

The experiments were performed in an electrochemical cell containing 1 mol/L sulfuric acid with 0.5 mm diameter iron working, Hg/Hg_2SO_4 sat. K_2SO_4 reference, and Pt counter electrodes. At constant circuit potential $V = -0.20$ V with respect to the reference electrode, the current of each wire $I(t)$ can be measured. (The data acquisition rate was 1000 Hz.) The 2-electrode experiments generated time series data of 60 s–120 s and the 25-electrode measurements of 50 s. (The two-electrode measurements could be performed longer because it was easier to maintain the quasistationary chaotic dynamics for 2 electrodes than for 25 due to inherent heterogeneities in the surface conditions.)

The electrodes were connected to the potentiostat through individual parallel resistors (R_{ind}) and one series collective resistor (R_{coll}) in such a way that the total resistance $R_{\text{tot}} = R_{\text{ind}} + N_{el}R_{\text{coll}}$ was kept constant, but the collective resistance fraction $\epsilon = N_{el}R_{\text{coll}}/R_{\text{tot}}$ was changed; $N_{el} = 2$ or 25 is the number electrodes (or oscillators). As it was shown previously,[31] the collective resistance introduces global electrical coupling among the electrode potentials. The coupling is linear (potential differences generate coupling currents), has zero-delay, and thus expected to affect both the slow chaotic dynamics and the fast spiking. The strength of the coupling can be controlled with ϵ through adjustments of the individual and collective resistances. The coupling strength ϵ was varied between 0 (no coupling) and 1 (strong coupling).

The detailed description of this experimental setup was described in previous studies, where it was shown that the $I(t)$ presents two dynamics: The slow is chaotic and the fast exhibits irregular bursts of spiking.[18,30]

B. Wavelet transforms: Phase assignment and synchronization detection

Continuous or discrete wavelet transforms with complex basis have been reported as a useful tool to phase assignment for chaotic oscillators.[12–14,32]

A wavelet function is a square-integrable complex function $\psi(t)$ that has (i) zero mean and (ii) unitary energy in the Fourier sense. Given the function $\psi(t)$, we can define the continuous wavelet transform (CWT) of a one-dimensional time series $f(t)$, in time[33] and frequency[34] domains, by the equivalent expressions,

$$W_f^{\psi}(a,\tau) = k\int_{-\infty}^{\infty} f(t)\overline{\psi\left(\frac{t-\tau}{a}\right)}\,dt \tag{1}$$

and

$$W_{\hat{f}}^{\hat{\psi}}(a,\tau) = k^{-1}\int_{-\infty}^{\infty} \hat{f}(\omega)\overline{\hat{\psi}(a\omega)}\,\exp(-\imath\,\omega\tau)\,d\omega, \tag{2}$$

where $k = 1/a$ (or $1/\sqrt{a}$) is a normalization constant considering the L^1 (or L^2) norm, and $a > 0$ and τ are real numbers called scale and translation parameters. The notation $\overline{\psi(t)}$ indicates the conjugate of complex values $\psi(t)$; $\hat{f}(\omega)$ and $\hat{\psi}(a\omega)$ represent the Fourier transform of $f(t)$ and $\psi(t)$, respectively. Equations (1) and (2) are equivalent formulations of CWT. Therefore, the values $W_f^{\psi}(a,\tau)$ are called wavelet coefficients. We notice that the second formulation has advantages to numerical calculations because the point to

point product has a smaller computational cost when compared to the convolution in the time domain.

We considered the Morse wavelet, defined directly in frequency by

$$\psi(\beta,\gamma,\omega) = 2(e\gamma\beta)^{\beta/\gamma}\, U(\omega)\omega^{\beta} e^{-\omega^{\gamma}}, \tag{3}$$

where $U(\omega)$ is the Heaviside function and $\gamma = 3$ and $\beta = 20$ are typical values in which $\psi(\beta,\gamma,\omega)$ exhibits a frequency symmetric response with Gaussian behavior and whose bandwidth is very narrow and, therefore, appropriate to analyze highly periodic signals.[35–37]

From wavelet coefficients computed by Eq. (2) or Eq. (1), we can calculate the global wavelet spectrum defined for each scale value a and given by

$$G(a) = \int_{-\infty}^{\infty} |W_f^{\psi}(a,\tau)|^2\, d\tau = \int_{-\infty}^{\infty} |W^{\hat{\psi}}(a,\tau)|^2\, d\tau. \tag{4}$$

The phase assignment using the CWT is performed as follows: We identify the scale $a_{\max}$ whose spectrum $G(a)$ has global maximum and calculated the argument of complex wavelet coefficients to this fixed scale.[12,13] Explicitly, we make

$$\phi(\tau) = \arctan\left(\frac{Imag(\psi(a_{\max},\tau))}{Re(\psi(a_{\max},\tau))}\right). \tag{5}$$

The discrete approach to phase assignment is made using the dual-tree complex wavelet transform (DT-ℂWT).[38,39] Consider $x(t)$ a chaotic oscillator decomposed using DT-ℂWT with M decomposition levels. In this case, the phase is assigned considering the application of Eq. (5) of the wavelet coefficients present in the level J whose discrete wavelet spectrum exhibits the largest magnitudes.[29]

We need to make one adaptation of this method to phase assignment to investigate the synchronization between two chaotic oscillators $x_{1,2}(t)$: the decomposition level J used for the computation of the phase according to Eq. (5) must be the same for each oscillators, and, for this, we choose $J = \min\{J^1, J^2\}$, where $J^{1,2}$ is the decomposition level whose discrete wavelet spectrum has the largest magnitudes.[14]

We adopted the synchronization index R as a measure of synchronization. Considering two oscillators $x_{1,2}(t)$ whose one-dimensional time series has length N, the index R is given by[40]

$$R = \left|\frac{1}{N}\sum_{k=1}^{N} \exp\left(\imath\,\Delta\phi(k)\right)\right|, \tag{6}$$

where $\Delta\phi$ is the phase difference. We notice that an R value close to 1 indicates that $x_{1,2}(t)$ is fully synchronized, but in practice, a value larger than 0.5 can indicate PS.

III. METHODOLOGY

A. Separation of fast and slow dynamics

We have shown in previous work that fast and slow dynamics can be extracted from experimental data sets using wavelet techniques.[30] For this, the CWT Morse wavelet is calculated in each experimental current $I(t)$; based on the global wavelet spectrum, the slow and the fast sub-band frequencies are determined. The fast and slow approximations of the time series are obtained by the inverse of the wavelet transform from the corresponding sub-bands.[30] $I_{(slow)}(t)$ and $I_{(fast)}(t)$ denote each dynamics extracted from the measured current $I(t)$ (mA) for the given oscillator.

B. Synchronization of slow dynamics

We characterized the synchronization between slow dynamics using the phase differences of the slow phases $\phi^{I}_{1,2\,(slow)}(t)$ obtained from the slow approximations $I_{1,2\,(slow)}(t)$ using the DT-ℂWT method described in Sec. II B. The synchronization index is used as defined in Eq. (6) and denoted by R_{slow}.

C. Synchronization of fast dynamics

The characterization of synchronization for the fast dynamics is made considering the time intervals in which the burstings occurs simultaneously in the approximations $I_{1,2\,(fast)}(t)$, that is, considering the bursting overlaps and an additional restriction for length of the overlaps as described below; Fig. 1 illustrates the methodology.

Consider two-oscillator pairs with fast dynamics $I_{1\,(fast)}(t)$ and $I_{2\,(fast)}(t)$; for each of these are m and n bursting time intervals with T_p and T_q, $p = 1,2,\ldots,m$ and $q = 1,2,\ldots,n$.

Analyzing the time intervals T_p and T_q, we looked at the intersections T_k with $0 < k \leq \min\{m,n\}$ but discarding all intersections whose length is smallest than 50% of the smallest bursting that constitutes it. More precisely, if T_k as an intersection between two time intervals T_p and T_q, we only considered it if

$$\#T_k \geq 0.5 \cdot \min\{\#T_p, \#T_q\}, \tag{7}$$

where the notation $\#T$ indicates the length of interval T. This overlap restriction is necessary to eliminate small overlapping intervals whose phase analysis is troublesome.

Let B_{over} be the set, whose elements are all intervals (T_k) for which the condition (7) is true. In these overlapping intervals, the current time series are denoted as $I^{over}_{1,2\,(fast)}(t)$ (outside the interval, these approximations are set to zero).

The phases $\phi_{1,2}(t)$ are assigned to $I^{over}_{1,2\,(fast)}(t)$ as described in Sec. II using the CWT with a Morse wavelet. As fast dynamics have relevance only in the time intervals T_k, the phases $\phi_{1,2}(t)$

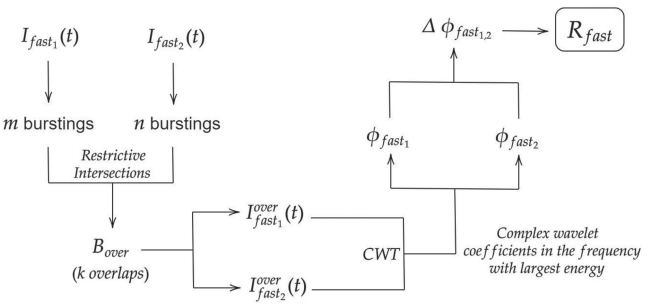

FIG. 1. General scheme to calculate the extent of synchronization of the fast subsystem (R_{fast}).

are restricted to these intervals. For data analysis purposes, the phases in the intervals are concatenated. This way, the fast phases $\phi_{1,2\,(fast)}$ represent the simultaneous occurrence of fast dynamics in the approximations $I_{1,2\,(fast)}(t)$.

As a synchronization measure for the fast dynamics, the R index given by Eq. (6) was modified by the introduction of a factor related to the number of burstings and overlaps as defined by

$$R_{fast} = \frac{k}{\min\{m,n\}} \left| \frac{1}{N} \sum_{k=1}^{N} \exp\left(\imath \Delta\phi_{1,2\,(fast)}(k)\right) \right|. \tag{8}$$

When the fast dynamics are fully synchronized, we have $k = \min\{m,n\}$. Therefore, in this case, the R_{fast} index reduces to R index as defined by Eq. (6). When the fast dynamics fully desynchronized, $k = 0$ because the set B_{over} is empty and R_{fast} index is zero.

IV. RESULTS AND DISCUSSION

In this section, we present the results of the synchronization analysis with 2 (Sec. IV A) and 25 (Sec. IV B) oscillators.

A. Synchronization of two oscillators

The currents of two uncoupled oscillators ($\epsilon = 0.0$) are shown in Figs. 2(a) and 2(b); for better visualization, only the initial 10 s are plotted. [For visual inspection, the repeated occurrence of the spiking waveforms is shown in Fig. 2(c) for Oscillator 2 on a shorter timescale; the shapes of these fast spiking waveforms were analyzed previously.[18]] A zoom to slow and fast dynamics approximations is shown in the bottom panels [Figs. 2(d) and 2(e), respectively]. As expected, the oscillations of both dynamics are asynchronous; particularly, notice that the bursting occurs in a different time interval.

In comparison, Fig. 3 shows the behavior with the strongest coupling, $\epsilon = 1.0$. Both the slow and fast dynamics nearly overlap, and the bursting occurs in the same intervals. These observations confirm the presence of nearly identical synchronization of the MTSDS oscillators. Next, we quantified the transition from no synchrony to full synchrony, as the coupling strength was increased based on the phase differences of the slow and fast approximations and the fraction of the overlapping bursting intervals.

1. Synchronization of the slow dynamics

For the synchrony analysis, we have calculated the slow phases for both oscillators; as previously discussed,[30] the slow phases correspond to levels 7 or 8 of the discrete wavelet transform. (The more dominant level was selected for a given analysis.)

The slow phase differences (top) and the corresponding cyclic phase difference probability density distributions (middle) are shown in Fig. 4 for coupling strengths $\epsilon = 0.0$, 0.6, 0.8, and 1.0.

For $\epsilon = 0.0$ and 0.6, there is no PS: The phase differences increase nearly linearly, and the corresponding distributions are flat. (Similar behavior was seen with $\epsilon = 0.7$.) For $\epsilon = 0.8$, there is intermittent synchrony with time periods with constant phase differences, which are interrupted by phase divergence; the histogram shows a preferred phase difference close to 0 (or 2π). Finally, for $\epsilon = 1.0$, the phase difference vs time plot is dominated by constant values with multiple of 2π values interrupted by very quick jumps; the histogram shows phase locking behavior with phase difference close to zero.

The synchronization index R_{slow} vs ϵ graph is shown in Fig. 5(c). The values of the R index are smaller than 0.30 with $\epsilon \leq 0.7$ and are larger than 0.6 for $\epsilon \geq 0.8$. Notice that the value of the R_{slow} index sharply increases when the coupling strength changes from $\epsilon = 0.7$ to 0.8.

These observations indicate that PS of the slow dynamics emerges for $\epsilon > 0.7$, and it is relatively quick transition. In comparison, previous experiments[41] with phase coherent electrochemical oscillators (with nickel dissolution) showed PS at relatively weak coupling strength ($\epsilon \approx 0.1 - 0.2$). Non-phase coherent chaotic electrodissolution with iron (without bursting), similar quick transition was observed with strong coupling ($\epsilon \approx 0.4 - 0.6$).[41] The results thus show that the slow dynamics of the chaotic iron dissolution system with bursting showed similar transition to phase synchrony as without bursting, but at somewhat larger coupling strength.

2. Synchronization of the fast dynamics

a. Bursting occurrence rate, regularity, and overlap. Synchronization of the fast spiking oscillations is only possible when the bursting intervals overlap. Therefore, before analysis of the fast spiking synchronization, it is useful to explore how often the fast spiking occurs and what is the length of such bursting events.

Figure 5(a) shows the number of bursting intervals divided by the length of the time series. Without coupling, the two oscillators show different rates, about 0.25 and 1.0 s^{-1}. This measurement further confirms that there are structural heterogeneities in the two oscillators with one producing more bursting events than the other. As the coupling was increased, the average bursting rate of the oscillator first decreased and for stronger coupling ($\epsilon > 0.6$) increased again. For the strongest coupling ($\epsilon = 1.0$), both oscillators have the same bursting rate of about 0.5 s^{-1}.

In addition to an occurrence rate of the bursting, their length also changed. Figure 6(a) shows the histograms of the bursting lengths. Without coupling, the two oscillators have bursting lengths of 0.13 and 0.10 s with a standard deviation of 0.026 and 0.012 s, respectively. With strong coupling [$\epsilon = 1.0$, see the histogram in Fig. 6(b)], the average length and standard deviations are the same for both oscillators, 0.08 and 0.011 s, respectively. Note that the length of the bursting interval of one of the oscillators now has a smaller standard deviation, which is an indication of a bursting regularization phenomenon induced by the coupling.

As the coupling strength is increased, more and more bursting intervals overlap. Figure 5(b) shows the fraction of overlapping bursting intervals as a function of the coupling strength. For coupling strength $\epsilon \leq 0.4$, most of the bursting intervals do not overlap (fraction of overlapping burstings is less than 0.5). However, for $\epsilon \geq 0.8$, most (larger than 80%) of the bursting intervals overlap.

b. Synchronization of fast spiking. Even for weak coupling, some bursting intervals overlap, and thus, the extent of synchronization can be calculated for each coupling strength.

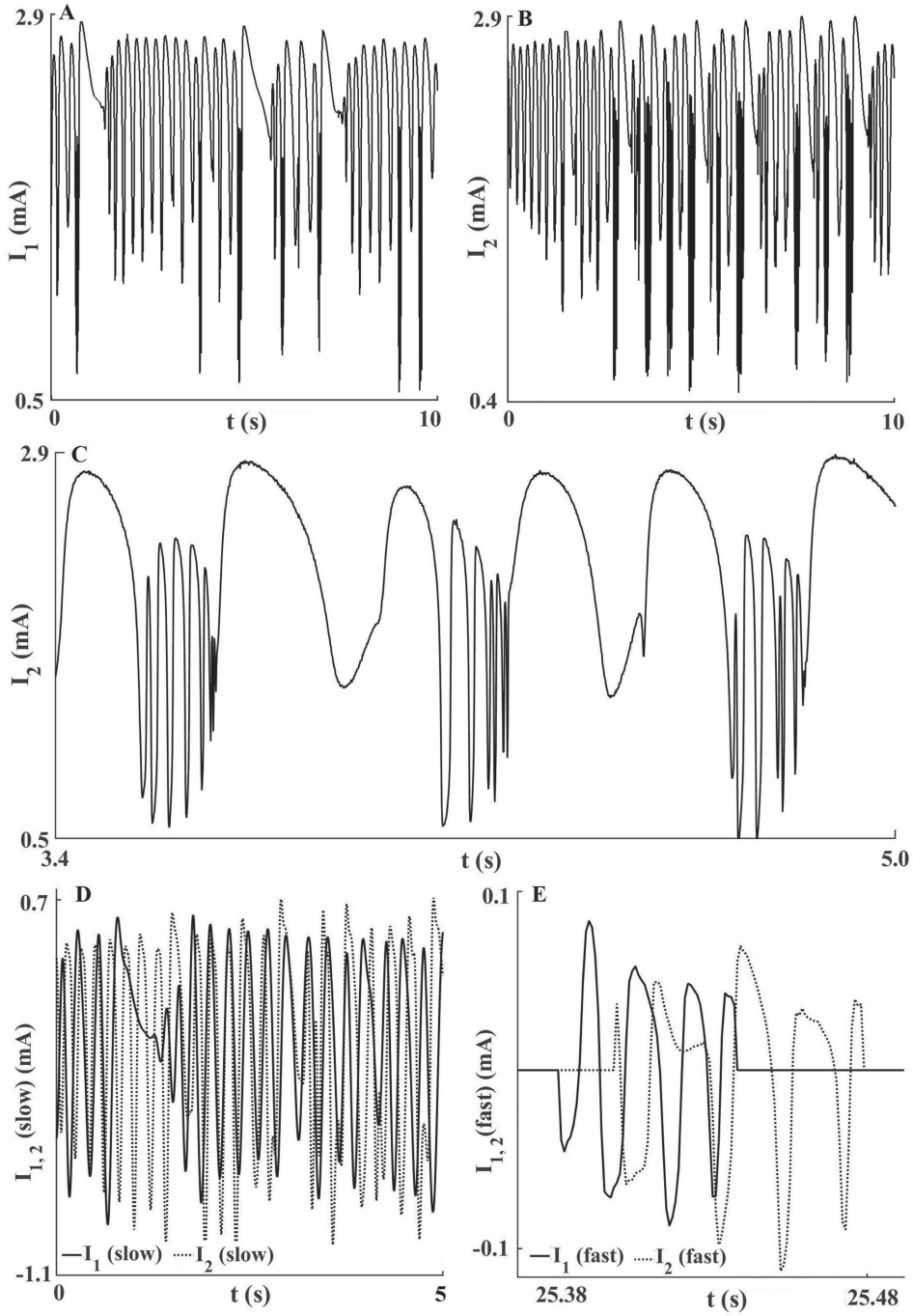

FIG. 2. Desynchronized current time series of two uncoupled ($\epsilon = 0.0$) chaotic bursting oscillators. (a) Oscillator 1 [$I_1(t)$]. (b) Oscillator 2 [$I_2(t)$]. (c) Three consecutive bursting events of Oscillator 2. Bottom panels: Approximations to slow (d) and fast dynamics (e).

Figure 7(a) shows the time series of such a bursting interval for $\epsilon = 0.0$. There is no coupling, and the two overlapping bursting intervals show oscillations typically seen for desynchronized systems. The phase differences [Fig. 7(d)] obtained from the fast phases [Fig. 7(c)] increase nearly linearly with time. However, in the strongly coupled case [$\epsilon = 1.0$, Figs. 7(b), 7(e), and 7(f)], the oscillations nearly overlap, and the phase difference is mostly horizontal lines at multiples of 2π corresponding to in-phase synchronization.

By collection of the phase differences for bursting intervals, the fast synchronization index can be calculated for each coupling strength; see Fig. 5(c). For $\epsilon < 0.7$, there is little synchrony

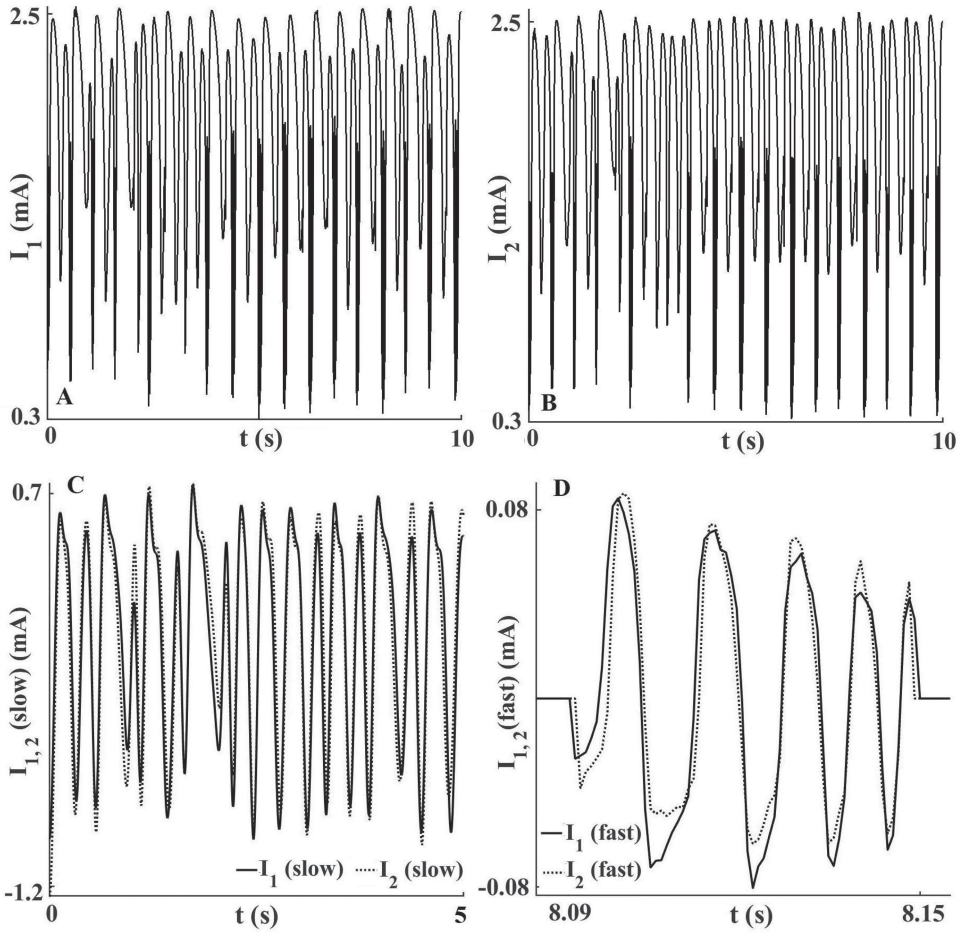

FIG. 3. Synchronized current time series of two strongly coupled ($\epsilon = 1.0$) chaotic bursting oscillators. (a) Oscillator 1 [$I_1(t)$]. (b) Oscillator 2 [$I_2(t)$]. Bottom panels: Approximations to slow (c) and fast dynamics (d).

($R_{fast} < 0.25$), and the behavior is similar to the $\epsilon = 0.0$ case. However, for $\epsilon \geq 0.7$, nearly all bursting intervals are synchronized ($R_{fast} > 0.8$). Therefore, there is sudden transition to full bursting synchronization at a coupling strength of $\epsilon = 0.7$.

3. Synchronization transitions: Summary

In summary, the analysis showed rich dynamics in transition to fully synchrony. For weak coupling, $\epsilon < 0.6$, neither the slow dynamics nor the fast spiking is synchronized, and the bursting intervals do not overlap. At $\epsilon = 0.6$, the fast bursting intervals overlap without any synchrony. At $\epsilon = 0.7$, the fast spiking synchronizes without synchronization of the slow oscillations. This state is similar to those reported with slow–fast Hindmarsh–Rose oscillator networks.[25] Finally, at $\epsilon = 0.8$, the slow system also synchronizes.

B. Synchronization of 25 oscillators

In this section, the results about the characterization of synchronization with 25 globally coupled oscillators are presented.

1. Synchronization of the slow dynamics

Figures 8(a)–8(c) show the behavior without coupling ($\epsilon = 0.0$). The single oscillator time series [Fig. 8(a)] look similar to those observed with the two oscillators in Fig. 2(a): The slow chaotic behavior is interrupted with fast spiking bursts. The time series of the slow approximations in a space-time grayscale plot is shown in Fig. 8(b); there is no apparent structure that would indicate a spatial structure. The R_{slow} indices for all oscillator pairs are shown in Fig. 8(c); all the values are small ($R_{fast} < 0.25$), which further confirms the lack of synchronization for the uncoupled case.

The behavior with the strongest coupling ($\epsilon = 1.0$) is shown in Figs. 8(d)–8(f). The time series data [Fig. 8(d)] reveal a surprising feature: The bursts completely disappear, and thus, the slow dynamics is equivalent to the original time series in the case. The space-time plot of the currents of the oscillators [Fig. 8(e)] now shows correlated structures with very similar variations. The high level of synchronization is further confirmed by the R_{slow} matrix

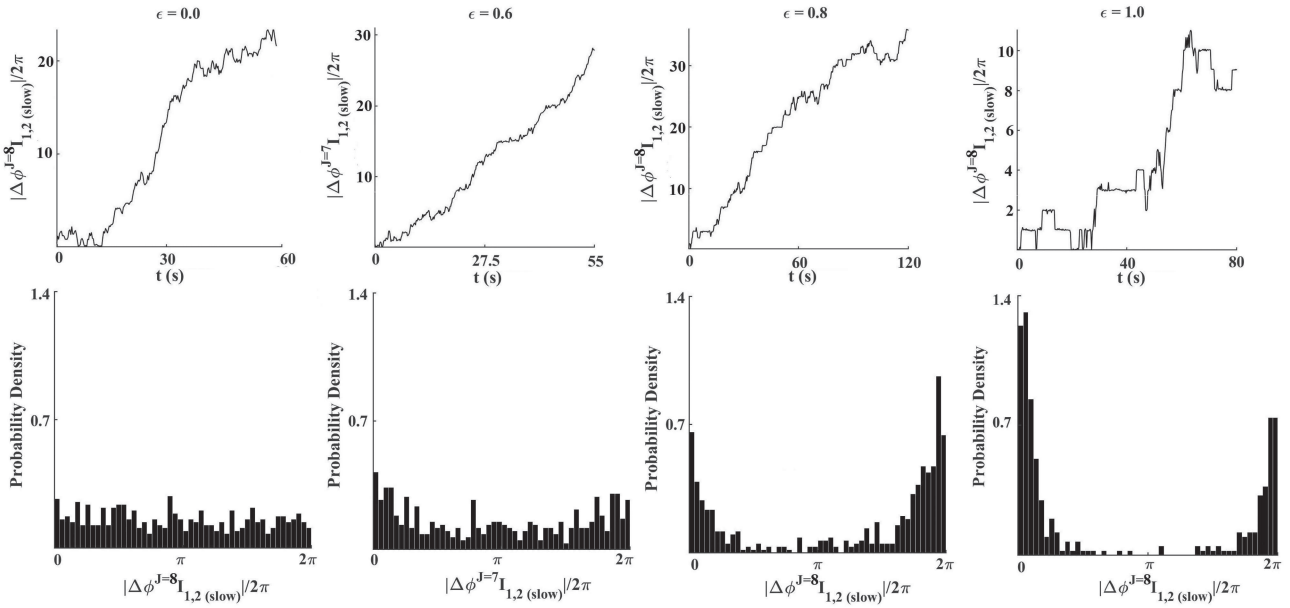

FIG. 4. Phase synchronization of the slow dynamics of two coupled chaotic bursting oscillators. Slow phase differences (top row) and probability density histograms (bottom row) with $\epsilon = 0.0,\ 0.6\ ,\ 0.8\ ,$ and 1.0.

in Fig. 8(f) with large values ($R_{slow} > 0.6$) for each oscillator pairs. Therefore, the oscillations exhibit high level of synchronization with $\epsilon = 1.0$.

The R_{slow} indices and their mean for each coupling strengths are shown in Fig. 9(b). For $\epsilon \leq 0.4$, the mean R_{slow} values are low (about 0.1); with a further increase of the coupling, there is a transition to PS. For $\epsilon = 0.6$, some oscillator pairs are desynchronized ($R_{slow} < 0.5$) and some are synchronized ($R_{slow} > 0.5$); note that there are a large number of oscillator pairs at the border of synchronization; i.e., $R_{slow} \approx 0.5$. The situation is similar with more synchronized pairs for $\epsilon = 0.80$. Finally, the population is fully synchronous for $\epsilon = 1.0$. The overall picture of this synchronization transition is similar to the second order phase transition observed with globally coupled, weakly heterogeneous phase coherent chaotic electrochemical oscillators.[42]

2. Fast dynamics

Figure 9(a) shows the bursting occurrence rate as a function of the coupling strength. Bursting oscillations occur only for weak coupling ($\epsilon = 0.0$ and 0.20), with relatively large heterogeneities across the populations. We thus see that the main effect of coupling on the fast dynamics is the disappearance of bursting oscillations, which can also be regarded as coupling induced regularization

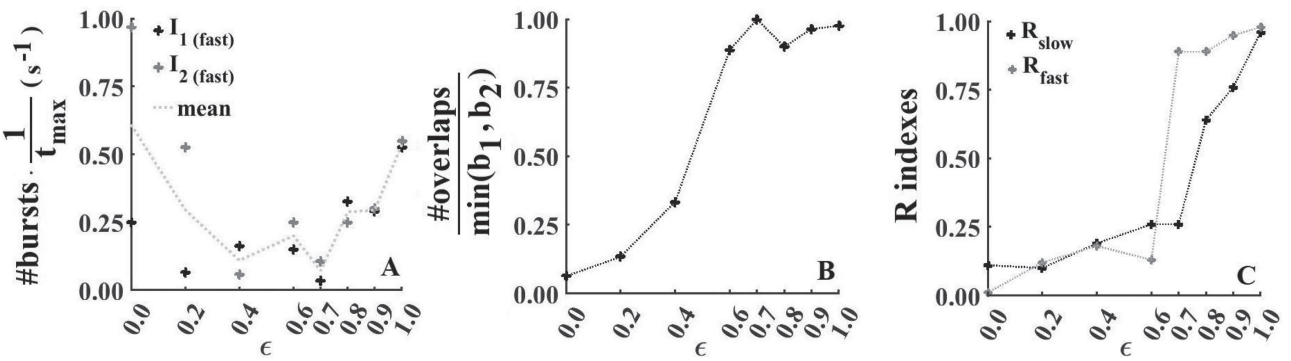

FIG. 5. Synchronization analysis of two coupled oscillators. Bursting occurrence rates (a) and bursting overlaps (b) as a function of coupling strength (ϵ). (c) The slow (R_{slow}) and fast (R_{fast}) phase synchronization indices as a function of the coupling strength.

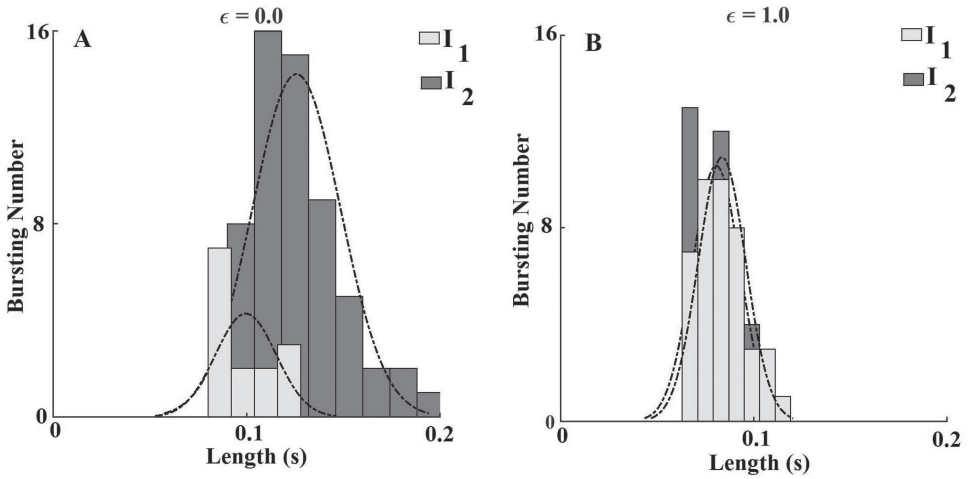

FIG. 6. Histograms of bursting interval lengths for two uncoupled [$\epsilon = 0.0$, panel (a)] and strongly coupled [$\epsilon = 1.0$, panel (b)] oscillators.

phenomena: For strong coupling, the complexity of the time series greatly reduces by completely eliminating the fast scales. A qualitative explanation for such behavior could be related to the fact that complete synchronization in networks of a multiple time-scale system is difficult to achieve.[27] Qualitatively, the emergence of bursting oscillations requires well-timed feedback loops; with relatively large heterogeneities, the strong coupling can destroy the subtle timing of the loops and the system cannot enter the phase space region for bursting oscillations simultaneously.

V. CONCLUSIONS

Analysis of a coupled pair and population electrochemical oscillators that exhibited chaotic slow and periodic fast spiking

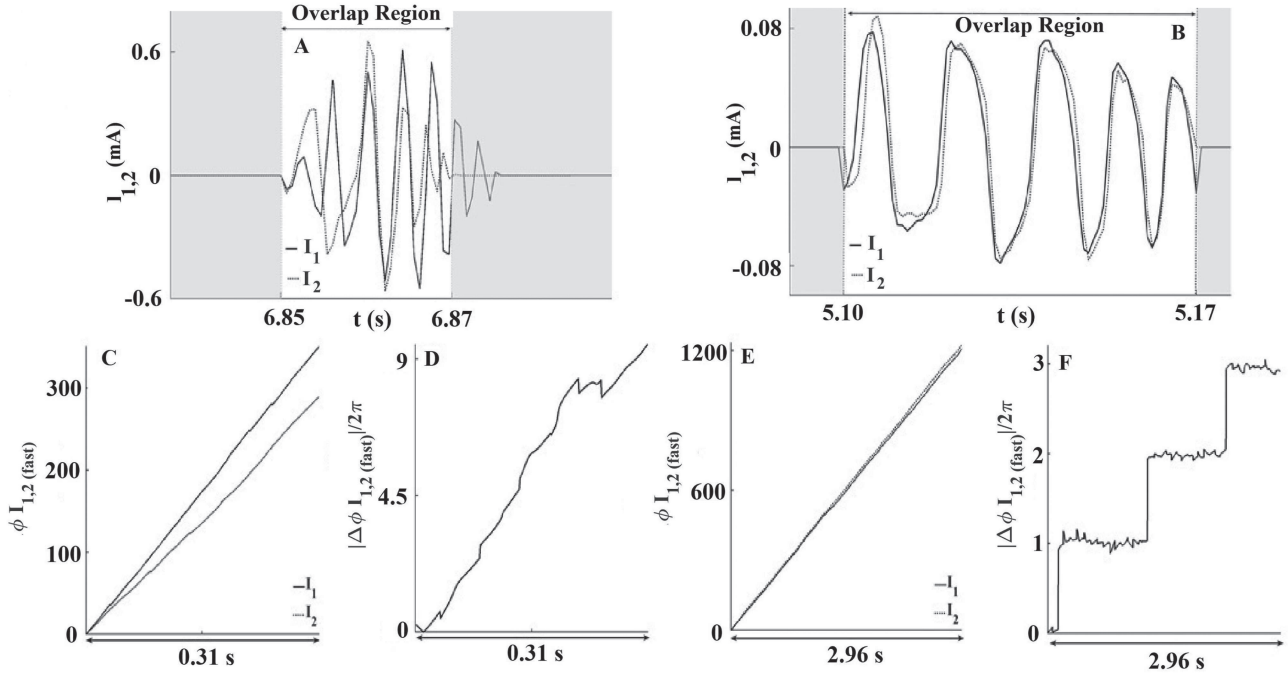

FIG. 7. Fast dynamics synchronization of two coupled oscillators. Top row: A representative bursting overlap without [$\epsilon = 0.0$, (a)] and with strong [$\epsilon = 1.0$, (b)] coupling. Bottom row: Fast phases and their difference for $\epsilon = 0.0$ (c) and (d) and $\epsilon = 1.0$ (e) and (f).

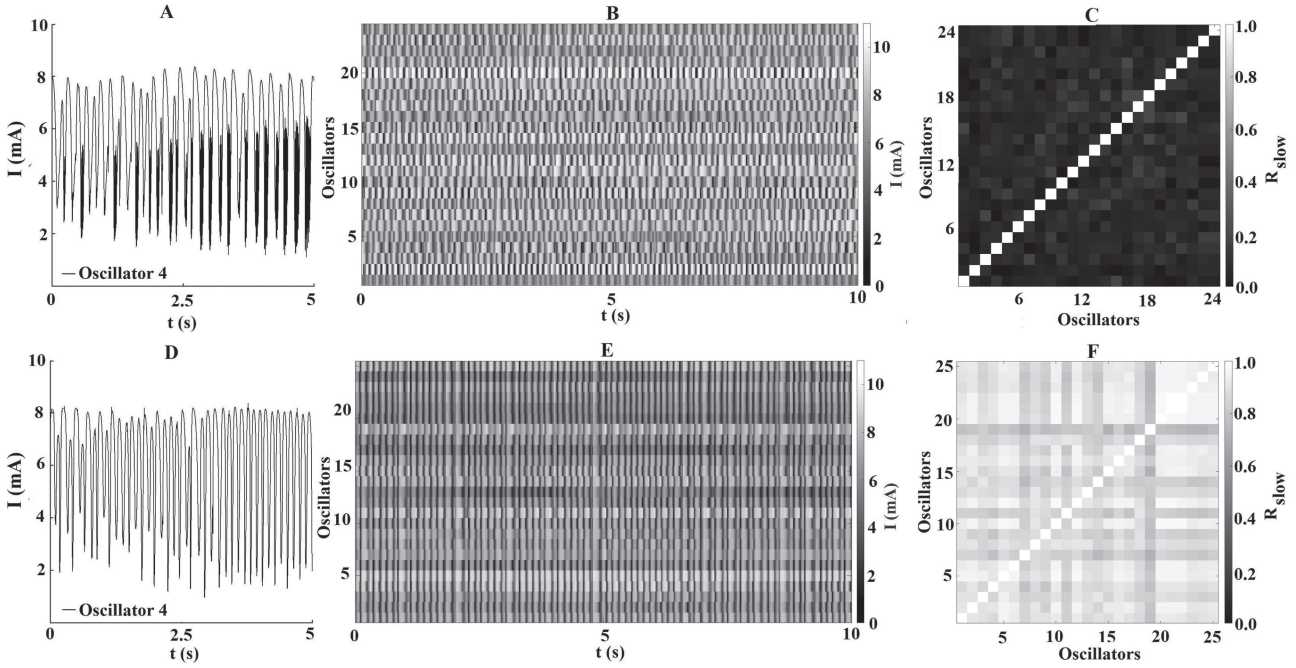

FIG. 8. Synchronization of a population of chaotic bursting oscillators. Current time series of a representative oscillator [left, panels (a) and (d)], space-time grayscale plots of the currents of the slow approximations [middle, panels (b) and (e)], and the slow synchronization index matrix, R_{slow} [right, panels (c) and (f)]. Top row: Uncoupled oscillators ($\epsilon = 0.0$). Bottom row: Strongly coupled oscillators ($\epsilon = 1.0$).

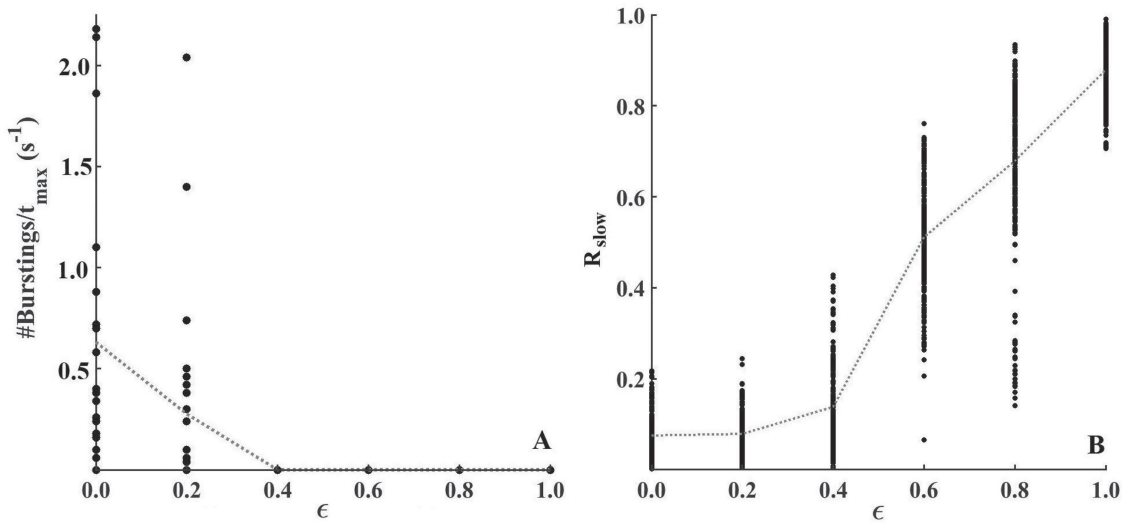

FIG. 9. Bursting occurrence rate (a) and slow synchronization indices (b) as a function of coupling strength for the population of oscillators. Dashed lines indicate the mean values.

behavior revealed a rich transition to the fully synchronized state. Wavelet transform methods allowed separation of the dynamics into fast and slow, and synchronization measures could be constructed for the two timescales separately.

The two-oscillator system exhibited a progressive transition to synchronization: First, the bursting intervals overlapped, then the fast spiking oscillations synchronized, and finally, the slow chaotic dynamics synchronized. For the globally coupled population, the fast spiking disappeared with increasing the coupling strength, which was followed by synchronization of the slow dynamics. This difference in the behavior may be related to the effect of dynamical heterogeneities of the oscillators. With two electrodes, it was relatively easy to obtain similar chaotic bursting dynamics, and thus, the slow and fast subsystems could synchronize. However, with 25 oscillators, the heterogeneities were stronger, and bursting synchronization did not occur. As such, it could be expected that it is the extent of heterogeneities, and not the number of oscillators, the determining factor. In general, the oscillators can exhibit heterogeneities inherently present (metal impurity, electrode size) or being developed (O_2 bubbles, pitting corrosion, surface oxide thickness, and porosity) during the course of the reaction; experimental techniques to control these heterogeneities could be required for better characterization of the synchronization dynamics.

In previous studies,[25,27] bursting oscillations systems were considered with one-variable slow dynamics. In these studies, the synchronization of the slow subsystem (which coincided with bursting intervals overlaps) preceded the synchronization of the fast system. Note, however, that in the presented experimental system, the slow subsystem is chaotic;[18] according to the results, in such a higher dimensional slow subsystem, overlapping bursting intervals can occur without PS of slow chaotic oscillations.

The results have implications in other systems, in particular, neural oscillations, where typically one-dimensional time series are available for each oscillator and multiple timescales exist that can interact with each other. The presented experimental results can also initiate further theoretical studies for bursting oscillations with slow timescales that are governed by more than one variable and thus can generate complex dynamics. For example, the kinetic model for periodic bursting in iron electrodissolution[43] could be extended to account for the chaotic behavior or a phenomenological model with a combination of automated attractor state space,[44] and global vector field reconstruction[45] techniques could be used to explore the bifurcations underlying the experimentally observed synchronization effects.

ACKNOWLEDGMENTS

L.A.M. received financial support from the Coordenação de Aperfeiçoamento de Pessoal de Nível Superior—Brazil (CAPES)—Finance Code 001 and is grateful for discussions about this work with Juliana C. Lacerda. M.O.D. acknowledges the financial support from the Conselho Nacional de Desenvolvimento Científico e Tecnológico (CNPq) (Grant Nos. 302226/2018-4 and 2020/13015-0) and the São Paulo Research Foundation (FAPESP) (Grant No. 2015/25624-2). E.E.N.M. is supported by Grant No. 2015/50122-0 of the São Paulo Research Foundation (FAPESP) and Grant No. 307714/2018-7. I.Z.K. acknowledges support from the National Science Foundation CHE-1900011 grant.

DATA AVAILABILITY

The data that support the findings of this study are available from the corresponding author upon reasonable request.

REFERENCES

[1] A. Tyrrell, G. Auer, and C. Bettstetter, "Fireflies as role models for synchronization in ad hoc networks," in *2006 1st Bio-Inspired Models of Network, Information and Computing Systems* (IEEE, 2006), pp. 1–7.
[2] Z. Néda, E. Ravasz, T. Vicsek, Y. Brechet, and A. Barabási, "Physics of the rhythmic applause," Phys. Rev. E **61**, 6987–6992 (2000).
[3] R. Ims and H. P. Andreassen, "Spatial synchronization of vole population dynamics by predatory birds," Nature **408**, 194–196 (2000).
[4] A. Pikovsky, J. Kurths, and M. Rosenblum, *Synchronization: A Universal Concept in Nonlinear Sciences* (Cambridge University Press, 2003).
[5] T. Yamada and H. Fujisaka, "Stability theory of synchronized motion in coupled-oscillator systems: The mapping approach," Prog. Theor. Phys. **70**, 1240–1248 (1983).
[6] A. S. Pikovsky and P. Grassberger, "Symmetry breaking bifurcation for coupled chaotic attractors," J. Phys. A **24**, 4587–4597 (1991).
[7] M. G. Rosenblum, A. S. Pikovsky, and J. Kurths, "Phase synchronization of chaotic oscillators," Phys. Rev. Lett. **76**, 1804–1807 (1996).
[8] A. S. Pikovsky, M. G. Rosenblum, and J. Kurths, "Synchronization in a population of globally coupled chaotic oscillators," Europhys. Lett. **34**, 165–170 (1996).
[9] A. Goryachev and R. Kapral, "Spiral waves in chaotic systems," Phys. Rev. Lett. **76**, 1619–1622 (1996).
[10] A. Pikovsky, M. Zaks, M. Rosenblum, G. Osipov, and J. Kurths, "Phase synchronization of chaotic oscillations in terms of periodic orbits," Chaos **7**, 680–687 (1997).
[11] C. Chandre, S. Wiggins, and T. Uzer, "Time–frequency analysis of chaotic systems," Physica D **181**, 171–196 (2003).
[12] A. A. Koronovskii and A. E. Hramov, "Chaotic phase synchronization studied by means of continuous wavelet transform," Tech. Phys. Lett. **30**, 587–590 (2004).
[13] A. E. Hramov and A. A. Koronovskii, "Time scale synchronization of chaotic oscillators," Physica D **206**, 252–264 (2005).
[14] M. T. Ferreira, R. Follmann, M. O. Domingues, E. N. Macau, and I. Z. Kiss, "Experimental phase synchronization detection in non-phase coherent chaotic systems by using the discrete complex wavelet approach," Chaos **27**, 083122 (2017).
[15] M. Desroches, J. Guckenheimer, B. Krauskopf, C. Kuehn, H. M. Osinga, and M. Wechselberger, "Mixed-mode oscillations with multiple time scales," SIAM Rev. **54**, 211–288 (2012).
[16] E. M. Izhikevich, "Synchronization of elliptic bursters," SIAM Rev. **43**, 315–344 (2001).
[17] E. M. Izhikevich, "Simple model of spiking neurons," IEEE Trans. Neural Netw. **14**, 1569–1572 (2003).
[18] I. Z. Kiss, Q. Lv, L. Organ, and J. L. Hudson, "Electrochemical bursting oscillations on a high-dimensional slow subsystem," Phys. Chem. Chem. Phys. **8**, 2707–2715 (2006).
[19] X. Chen, M. Heidarinejad, J. Liu, and D. P. Christofides, "Composite fast-slow MPC design for nonlinear singularly perturbed systems," AIChE J. **58**, 1802–1811 (2012).
[20] Y. Wang and S. Boyd, "Fast model predictive control using online optimization," IEEE Trans. Control Syst. Technol. **18**, 267–278 (2010).
[21] H. Wang, Q. Wang, and Q. Lu, "Bursting oscillations, bifurcation and synchronization in neuronal systems," Chaos, Solitons Fractals **44**, 667–675 (2011).
[22] A. Karantonis, D. Koutsaftis, and N. Kouloumbi, "Single and coupled electrochemical bursters during the electrodissolution/passivation of iron," Electrochim. Acta **55**, 374–382 (2009).

[23]A. Karantonis, D. Koutsaftis, and N. Kouloumbi, "Synchronization properties of coupled electrochemical bursters," J. Appl. Electrochem. **40**, 989–995 (2010).
[24]N. F. Rulkov, "Regularization of synchronized chaotic bursts," Phys. Rev. Lett. **86**, 183–186 (2001).
[25]I. Omelchenko, M. Rosenblum, and A. Pikovsky, "Synchronization of slow-fast systems," Eur. Phys. J. Spec. Top. **191**, 3–14 (2010).
[26]M. V. Ivanchenko, V. G. Osipov, V. D. Shalfeev, and J. Kurths, "Phase synchronization in ensembles of bursting oscillators," Phys. Rev. Lett. **93**, 134101–134105 (2004).
[27]T. Pereira, M. S. Baptista, and J. Kurths, "Multi-time-scale synchronization and information processing in bursting neuron networks," Eur. Phys. J. Spec. Top. **146**, 155–168 (2007).
[28]L. Menezes, E. Parma, E. G. Machado, and R. Nagao, "Quasiperiodic behavior in the electrodeposition of Cu/Sn multilayers: Extraction of activation energies and wavelet analysis," Phys. Chem. Chem. Phys. **21**, 21057–21063 (2019).
[29]M. T. Ferreira, C. B. Nobrega, M. O. Domingues, and E. E. N. Macau, "The discrete complex wavelet approach to phase assignment and a new test bed for related methods," Chaos **25**, 013117 (2015).
[30]L. A. Magrini, M. O. Domingues, E. E. N. Macau, and I. Z. Kiss, "Extraction of slow and fast dynamics of multiple time scale systems using wavelet techniques," Chaos **30**, 31–39 (2020).
[31]I. Z. Kiss and J. L. Hudson, "Phase synchronization of nonidentical chaotic electrochemical oscillators," Phys. Chem. Chem. Phys. **4**, 2638–2647 (2002).
[32]A. Hramov, A. A. Koronovskii, V. Ponomarenko, and M. D. Prokhorov, "Detection of synchronization from univariate data using wavelet transform," Phys. Rev. E **75**, 056207 (2007).
[33]I. Daubechies, *Ten Lectures on Wavelets* (SIAM, 1992).
[34]J. Sadowsky, "The continuous wavelet transform: A tool for signal investigation and understanding," Johns Hopkins APL Tech. Dig. **15**, 306–318 (1994).
[35]S. C. Olhede and A. T. Walden, "Generalized Morse wavelets," IEEE Trans. Signal Proces. **50**, 2661–2670 (2002).
[36]J. M. Lilly and S. C. Olhede, "Generalized Morse wavelets as a superfamily of analytic wavelets," IEEE Trans. Signal Proces. **60**, 6036–6041 (2012).
[37]J. M. Lilly and S. C. Olhede, "On the analytic wavelet transform," IEEE Trans. Inf. Theor. **56**, 4135–4156 (2010).
[38]I. W. Selesnick, "Hilbert transform pairs of wavelet bases," IEEE Signal Process. Lett. **08**, 170–173 (2001).
[39]I. W. Selesnick, "The design of approximate Hilbert transform pairs of wavelet bases," IEEE Trans. Signal Process. **50**, 1144–1152 (2002).
[40]F. Mormann, K. Lehnertz, P. David, and C. E. Elger, "Mean phase coherence as a measure for phase synchronization and its application to the EEG of epilepsy patients," Physica D **144**, 358–369 (2000).
[41]I. Z. Kiss, Q. Lv, and J. L. Hudson, "Synchronization of non-phase-coherent chaotic electrochemical oscillations," Phys. Rev. E **71**, 035201 (2005).
[42]Y. Kuramoto, *Chemical Oscillations, Waves, and Turbulence* (Courier Corporation, 2003).
[43]L. Organ, I. Z. Kiss, and J. L. Hudson, "Bursting oscillations during metal electrodissolution: Experiments and model," J. Phys. Chem. B **107**, 6648–6659 (2003).
[44]K. H. Kraemer, G. Datseris, J. Kurths, I. Z. Kiss, J. L. Ocampo-Espindola, and N. Marwan, "A unified and automated approach to attractor reconstruction," New J. Phys. **23**, 033017 (2021).
[45]C. Letellier, L. Le Sceller, P. Dutertre, G. Gouesbet, Z. Fei, and J. L. Hudson, "Topological characterization and global vector field reconstruction of an experimental electrochemical system," J. Phys. Chem. **99**, 7016–7027 (1995).